Special Feature: Nanomaterials and Processing

Nitrogen-functionalized Graphene Quantum Dots with Tunable Optical Properties

Hiroyuki Tetsuka, Akihiro Nagoya and Ryoji Asahi

▌**ABSTRACT**‖ Nitrogen-functionalized graphene quantum dots (NGQDs) with discrete molecular weights and specific edges, extracted from graphene sheets, glow with various bright colors, which are dependent on their edge functional groups, under single-wavelength excitation. The optical properties are precisely controlled by quantitative functionalization of the NGQDs, which results in a change of the resonance features between the delocalized orbital of graphene and the molecular orbital of the nitrogen-functional groups, as supported by MALDI-TOF mass analysis and density functional theory calculations. As an example, NGQDs with tunable optical properties are potentially applicable as color conversion materials for white light-emitting diodes (LEDs) through efficient incorporation into a flexible and transparent solid matrix. The NGQDs were incorporated into a flexible and transparent clay host using the electrostatic interactions among the cellulose nanofiber (CNF), NGQDs, and clay platelets. The resultant flexible NGQDs@CNF-clay hybrids with well organized structure exhibited bright colorful photoluminescence and were applied as a color conversion material for blue LEDs to achieve white light emission. The NGQDs@CNF-clay hybrid-based white LEDs have pure white light emission with a CIE coordinate of (0.33 0.37). These NGQDs and their hybrids are promising for use in a large array of future novel applications such as multicolor light-emitting devices, photovoltaics, photodetectors, bioimaging, biosensing, fuel cells, supercapacitors, and hydrogen production.

▌**KEYWORDS**‖ Graphene Quantum Dots, Graphene, Semiconductor, Clay Hybrids, White Light-emitting Diodes

1. Introduction

Graphene is an attractive material for use in photonics and optoelectronics due to its exceptional optical and electrical properties, such as strong broadband optical and saturable absorptivity.[1] In particular, the infrared response of graphene can be dynamically tuned by electrostatic gating, in contrast to conventional plasmonic materials. However, its application in the visible-light region is hindered, because graphene is a zero bandgap semiconductor. Recently, graphene quantum dots (GQDs), small graphene fragments, have been implemented in bandgap manipulation because of their quantum confinement and edge effects, which produce visible-light photoluminescence (PL). Luminescent GQDs with tunable emissions are regarded as next-generation nanomaterials to replace quantum dots composed of toxic and expensive semiconductor materials. Furthermore, their superior properties such as excellent solubility, stable PL, and biocompatibility make them promising candidates for future applications such as bio-imaging, photovoltaics, and light-emitting devices.[2-9]

Soluble luminescent GQDs can generally be prepared using solution chemistry approaches, either by top-down routes, where graphene sheet is cut through controlled oxidation or reduction processes,[3,5,7,8] or by bottom-up synthesis, where small precursor aromatic molecules are converted to larger molecules followed by oxidative exfoliation.[10] The presence of finite-sized molecular sp^2 domains and/or CO-related quasi-molecular fluorophores induced by the adsorption of oxygen functional groups can confine π electrons and consequently yield fluorescence that is determined by the nature of the sp^2 domains and functional groups.[11-13] However, despite their different oxidation states and scales, these GQDs exhibit similar blue fluorescence with a maximum centered at 420–450 nm, which is mainly ascribed to the limited tunability of the size and/or shape of sp^2 domains and

the adsorption of oxygen functional groups due to the insertion or removal of oxygen functional groups. To date, ideally tunable PL from GQDs has not yet been successfully achieved. Such tunability could be realized by enhancement of the homogeneity of the local electronic modifications of graphene by control of the sp^2 domain size, edge structure, and surface functional groups of GQDs. Here, we report on nitrogen-functionalized GQDs (NGQDs) with discrete molecular weights and specific edges, made from graphene sheets. The optical properties are precisely controlled only by the quantitative functionalization of GQDs. The NGQDs glow bright with various colors under single-wavelength excitation, the colors of which are dependent on their surface functional groups. The NGQDs were incorporated into a flexible and transparent clay host using the electrostatic interactions between the cellulose nanofiber (CNF) wrapped-NGQDs (NGQDs@CNF) and clay platelets. The resultant flexible NGQDs@CNF-clay films with well-organized structure were applied as a color conversion material for blue light-emitting diodes (LEDs) in an attempt to achieve white light emission.

2. Synthetic Methods

2. 1 Preparation of NGQDs

Oxidized graphene sheets (OGSs) were synthesized from graphite using the modified Hummers method. Typically, 5 mL of a water dispersion of OGSs was mixed with 8.0 mL of ammonia solution (19 wt% in water). After stirring for 30 min, the mixture was transferred to a poly (tetrafluoroethylene) (Teflon)-lined autoclave and heated at 70–150°C for 5 h. After cooling to room temperature, the large precipitated fragments were filtered out using a 0.02 μm membrane. The yellow supernatant was refluxed for 1 h to evaporate excess ammonia, and the obtained suspension was then further dialyzed for 5 days.

2. 2 Preparation of NGQDs@CNF-clay Films

CNF-wrapped NGQDs (NGQDs@CNF) were prepared by mixing a carboxylated CNF aqueous solution and an aqueous solution of NGQDs in a weight ratio of 0.1:1. The $Na_{0.22}[Mg_3][Al_{0.33}Si_{3.67}]O_{10}[OH]_2$ powder was mixed in water using a high shear mixer at a total solid concentration of 1 wt% with a 15 wt%

of NGQDs@CNF. The mixture was centrifuged at 5500 rpm and then poured onto a glass sheet in a mold. After drying, NGQDs@CNF-clay films with thicknesses of ca. 40 μm were peeled from the glass sheet.

2. 3 Instrumentation

X-ray photoelectron spectroscopy (XPS; Quantera SXM, Ulvac-Phi) measurements were performed using a monochromated Al Kα radiation source (100 μm spot diameter) at 1486.6 eV under high-vacuum conditions. X-ray diffraction (XRD; MXP18, Mac Science Ltd.) measurements were conducted using a Cu Kα source under an accelerating voltage of 40 kV and a current of 250 mA. Matrix-assisted laser desorption/ionization-time-of-flight (MALDI-TOF) mass spectra were recorded on a mass spectrometer (Autoflex, Bruker Daltonics, Germany) equipped with delayed extraction and a nitrogen laser (337 nm). In the positive reflectron mode, an accelerating voltage of 19.0 kV was used. Fourier-transform infrared spectroscopy (FT-IR; Nicolet MAGNA 760; Thermo Fisher Scientific, USA) was performed using the attenuated total reflection (ATR) method. Raman spectroscopy (NRS-3300, Jasco, Japan) was performed using the second harmonic of a Nd:YAG laser (λ = 532 nm). In addition, high-resolution transmission electron microscopy(HRTEM; JEM-2000EX, Hitachi) observations were performed at an accelerating voltage of 200 kV. Height profile measurements were conducted using atomic force microscopy (AFM; NanoscopeV D3100, Veeco Instruments). PL spectra were recorded using a spectrofluorometer (FP-6500; Jasco). PL quantum yields were measured using a quantum counter equipped with an integrating sphere (C9920-02, Hamamatsu). Luminescence spectra of NGQDs@CNF-clay based white LEDs (GWLEDs) were collected using a multi-channel spectrophotometer (USB4000; Ocean Optics Inc.). An integrating sphere was used in the assessment of luminous efficiency. The light conversion (blue-to-NGQDs emission) efficiency of the GWLEDs was calculated from the ratio of the number of photons emitted by the NGQDs to the total number of photons emitted from the blue LED and NGQDs.

2. 4 Ab Initio Calculations

The electronic structure of armchair-edged GQDs ($C_{36}H_{18}$) with various termination groups was calculated using the projector augmented wave (PAW) method as implemented in the Vienna ab initio simulation package (VASP). The exchange-correlation potential was treated using the generalized gradient approximation (GGA) with the Perdew, Burke, and Emzerhof parameterization. PAW data sets with radical cutoffs of 1.2 were employed using a plane-wave cutoff energy of 520 eV. The calculation was performed on a $20 \times 20 \times 10$ Å^3 unit cell.

3. Results and Discussions

Figure 1 shows a schematic illustration for the preparation of NGQDs from OGSs. The NGQDs were extracted from OGSs through the nucleophilic substitution reaction of oxygen-functional groups on OGSs with ammonia under amino-hydrothermal conditions. The formation of the NGQDs is dependent on the breakdown of nanometer domains of sp^2 carbon in the OGSs. OGSs have aromatic sp^2 domains of 2–3 nm in size isolated within a continuous sp^3 matrix of linearly aligned epoxy (–C-O-C–)-bonded sp^3 carbon atoms. The size of the sp^2 domains in the OGSs was calculated to be ca. 2.7 nm using the empirical Tuinstra–Koenig relationship,[14] which is based on the Raman D/G peak ratio. Under amino-hydrothermal treatment, ammonia reacts with epoxy groups on the OGS surfaces to form a primary amine and alcohols by nucleophilic substitution,[15,16] which enables extraction of the sp^2 domains by ring-opening of the epoxide and the simultaneous direct bonding of the primary amine with a graphene edge. In addition, a linear arrangement of epoxy bridges results in fragile OGSs due to the higher angular strain in the triangular rings, which leads to cleavage of the underlying C-C bonds. Consequently, size-controlled NGQDs that are edge-terminated with a primary amine are produced.

Figure 2(a) shows a comparison of the C 1s and N 1s XPS spectra from NGQDs and OGSs. The C 1s signal at 286.4 eV is assigned to epoxide groups, and the pronounced decrease in that peak is attributed to the loss of epoxides through nucleophilic reaction with ammonia. This interpretation is supported by the appearance of the N 1s signal at 399.7 eV, which
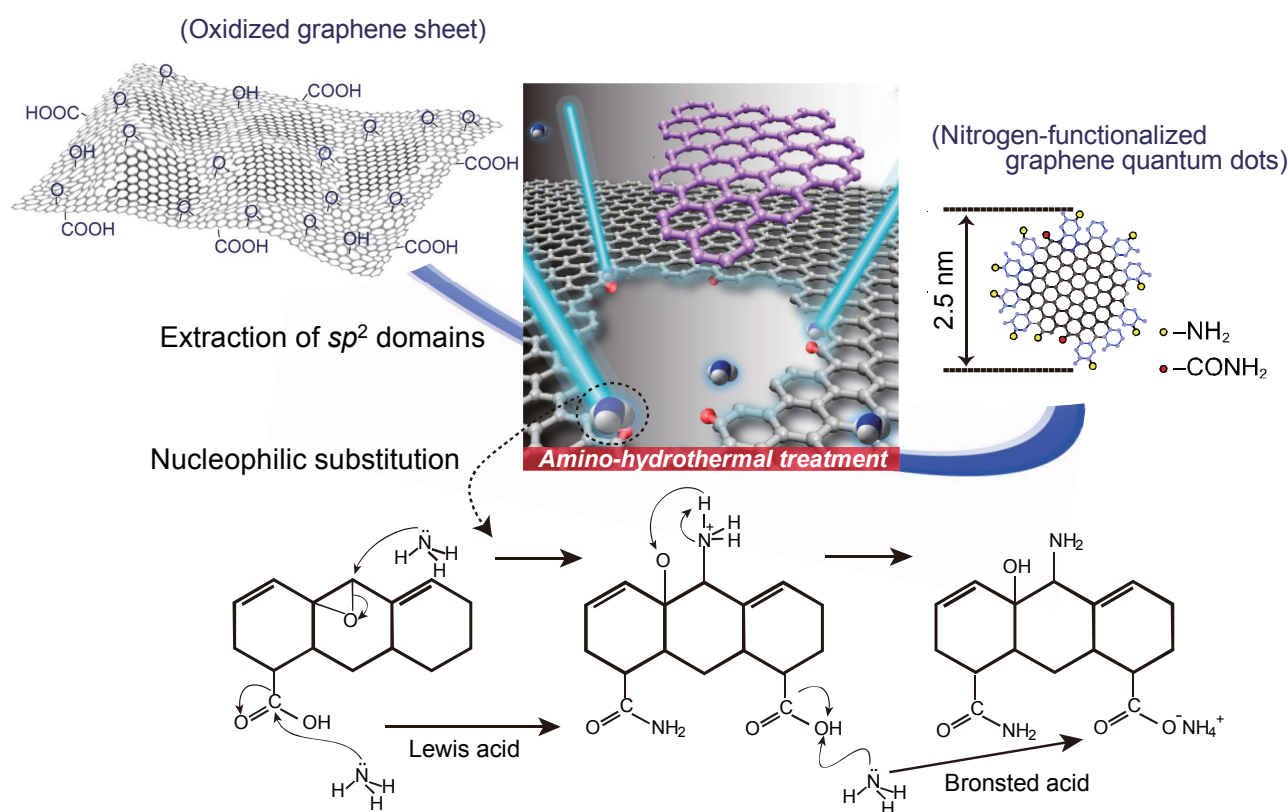

Fig. 1 Schematic illustration of the preparation of NGQDs using amino-hydrothermal treatment.

is assigned to primary amines (–NH$_2$). Successful functionalization with amine was also supported by FT-IR analysis (Fig. 2(b)). New FT-IR peaks at 1243 cm^{-1} (C-N in-plane stretching), 1617 cm^{-1} (N-H out-of-plane stretching), and 3300–3600 cm^{-1} (N-H in-plane stretching) from the amine groups appeared after amino-hydrothermal treatment. In addition, an amide-carbonyl (–NH-CO–) stretching vibration was also observed at 1650 cm^{-1}, which indicates the formation of amide groups through interactions with carboxylic groups as Lewis acids. The NGQDs have diameters of ca. 2.5 nm (**Fig. 3**(a)). A noticeable change in the size and shape of the NGQDs prepared at 70–120°C was observed. High temperature amino-hydrothermal treatment (>150°C) induced fragmentation of the NGQDs into smaller sizes. The inset of Fig. 3(a) shows clear (110) lattice fringes that indicate the high crystallinity of the NGQDs. AFM measurements verified that the NGQDs have a thickness of ca. 1.13 nm (Fig. 3(b)), which corresponds to a single layer of functionalized GQDs.[3,7,17] Figure 3(c) shows a Raman spectrum of the NGQDs. The relative intensity of the D/G bands is ca. 0.6, which is similar to that for electrochemically-derived GQDs[3,17] and graphene nanoribbons,[18,19] which implies the high quality of the NGQDs. The XRD pattern of the NGQDs has a weaker broad (002) peak than that for the OGSs centered at approximately $2\theta = 22.7°$ (Fig. 3(d)). The disappearance of the peak at $2\theta = 10.6°$ in the XRD for the NGQDs indicates the disordered stacking structures of individual graphene

layers and the absence of oxygen functional groups in the interlayers. The MALDI-TOF mass spectrum (Fig. 3(e)) revealed the narrow size distribution and unique edge structures of the NGQDs. Regular patterns with a repeating unit of m/z = 74 were observed between m/z = 1200 and 2500. This repeating unit of m/z = 74 is attributed to the reflection of the edge structure, where the mass of 74 is expected to be a six-membered carbon ring bonded to the armchair edge of an NGQD: 74 Δm = − [loss of two-coordinate six-membered carbon ring bonded to an armchair edge ($MW = 76$)] + [termination of two hydrogen atoms ($MW = 2$)], as shown in the inset of Fig. 3(e).

The NGQDs exhibit strong PL with a PL color change from blue to orange by functionalization with the primary amine.[20,21] **Figures 4**(a) and (b) show PL and excitation spectra and photographs of the emissions from the NGQDs. Aqueous suspensions of NGQDs exhibit bright colorful PL under a UV irradiation with a wavelength of 410 nm (Figure 4(b)). The corresponding PL and excitation peaks were red-shifted according to the quantity of amine functionalization in the range of 450–590 nm, and retained a sharp full-width-at-half-maximum (FWHM) as narrow as ca. 65–80 nm. The PL quantum yield was determined to be in the range of 29–1%, where a decrease was observed with a decrease in the quantity of amine functionalization. The different luminescence colors are considered to originate from the change in the electronic structure of the NGQDs. Ab initio calculations were performed using the plane-wave PAW method.[22,23] Based on the MALDI-TOF, FT-IR,
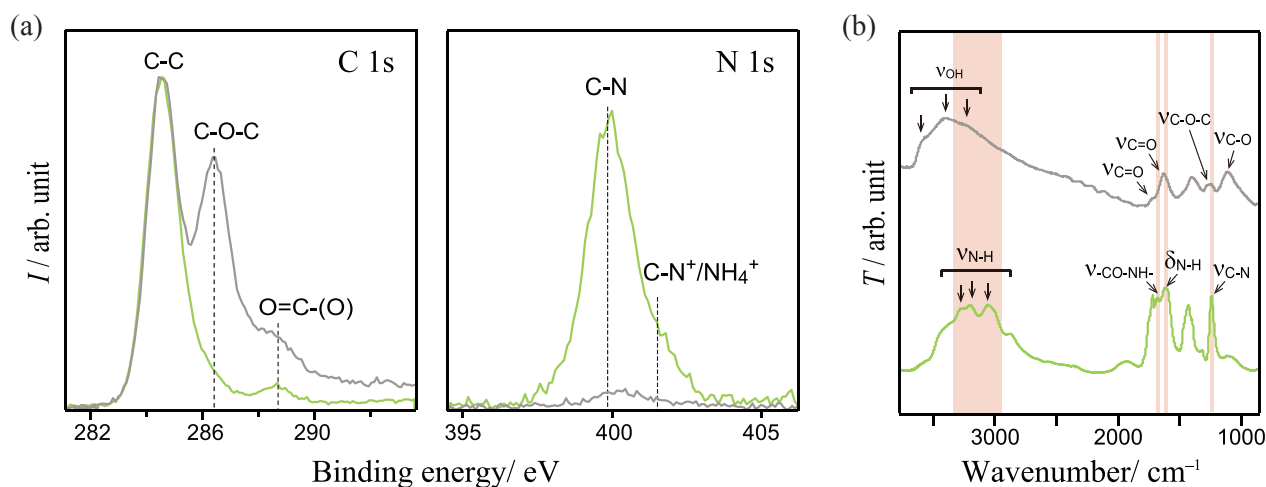

Fig. 2   (a) C 1s and N 1s XPS spectra for NGQDs prepared at 90°C (green line) and OGSs (gray line).
(b) FT-IR absorbance spectra for NGQDs prepared at 90°C (green line) and OGSs (gray line).

and XPS results, a graphene structure was modeled with two-coordinate six-membered carbon rings connected to armchair edges, as illustrated in Fig. 4(c). A primary amine alters the entire electronic structure of an NGQD; one degenerate highest occupied molecular orbital (HOMO) in the hydrogen-terminated graphene molecule is lifted to a higher energy in the NGQD as a consequence of strong orbital interaction with the primary amine. This interaction results in a narrowing of the optical bandgap. The resonance feature between the delocalized π orbital and the molecular orbital in the primary amine is thus the
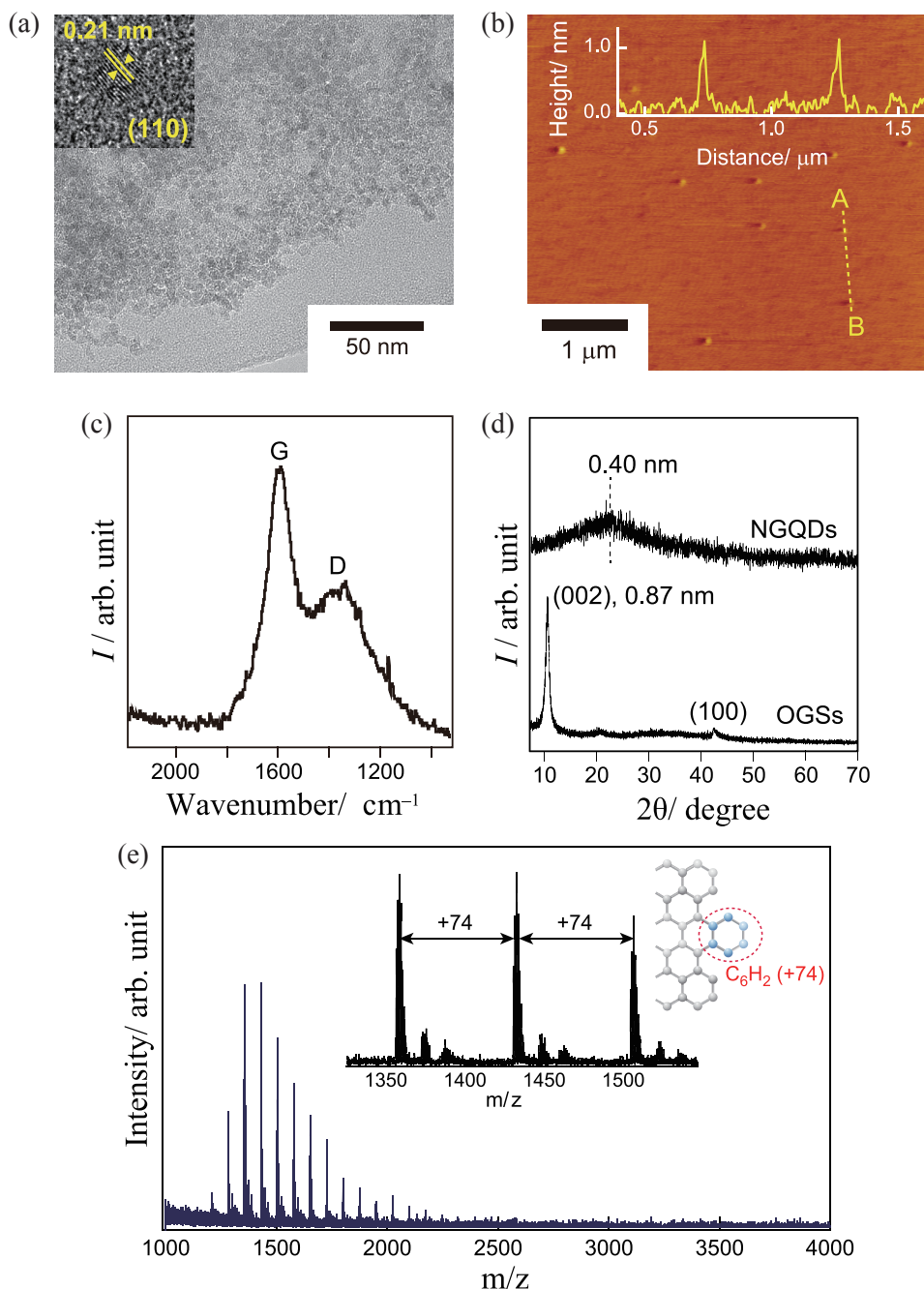
Fig. 3 (a) TEM image of the NGQDs prepared at 90°C. The inset shows the (110) lattice fringe. (b) AFM image of NGQDs prepared at 90°C on a mica substrate. The inset shows the height profile along the line A-B. (c) Raman spectrum of NGQDs prepared at 90°C. (d) XRD patterns of NGQDs prepared at 90°C and OGSs. (e) MALDI-TOF mass spectrum of NGQDs in aqueous solution prepared at 120°C. Note that peaks are detected as Na ion adducts ([M + Na]$^+$), the Na ion of which may have originated from residue in the reagents used for graphite oxidation to prepare the graphene oxide. The inset shows a schematic representation of the edge structure of the NGQDs.

origin of both the edge-treatment-dominated optical tunability and the high quantum efficiency. Such a resonant orbital can lead to intersystem crossing emission as a result of enhanced spin-orbital coupling. As such, extraordinarily long-delay luminescence of sub-second order (ca. 0.5 s) was observed from the NGQDs.

Stabilization of the NGQDs into a solid matrix is a crucial step that is necessary for their integration into solid-state devices. However, the PL properties of GQDs are closely correlated to the surface states; therefore, the stabilization of hydrophilic GQDs into a solid without the loss of their optical properties remains a challenge. We have previously examined the incorporation of NGQDs into flexible and transparent clay nanostructured films.[24-27] **Figure 5**(a) presents
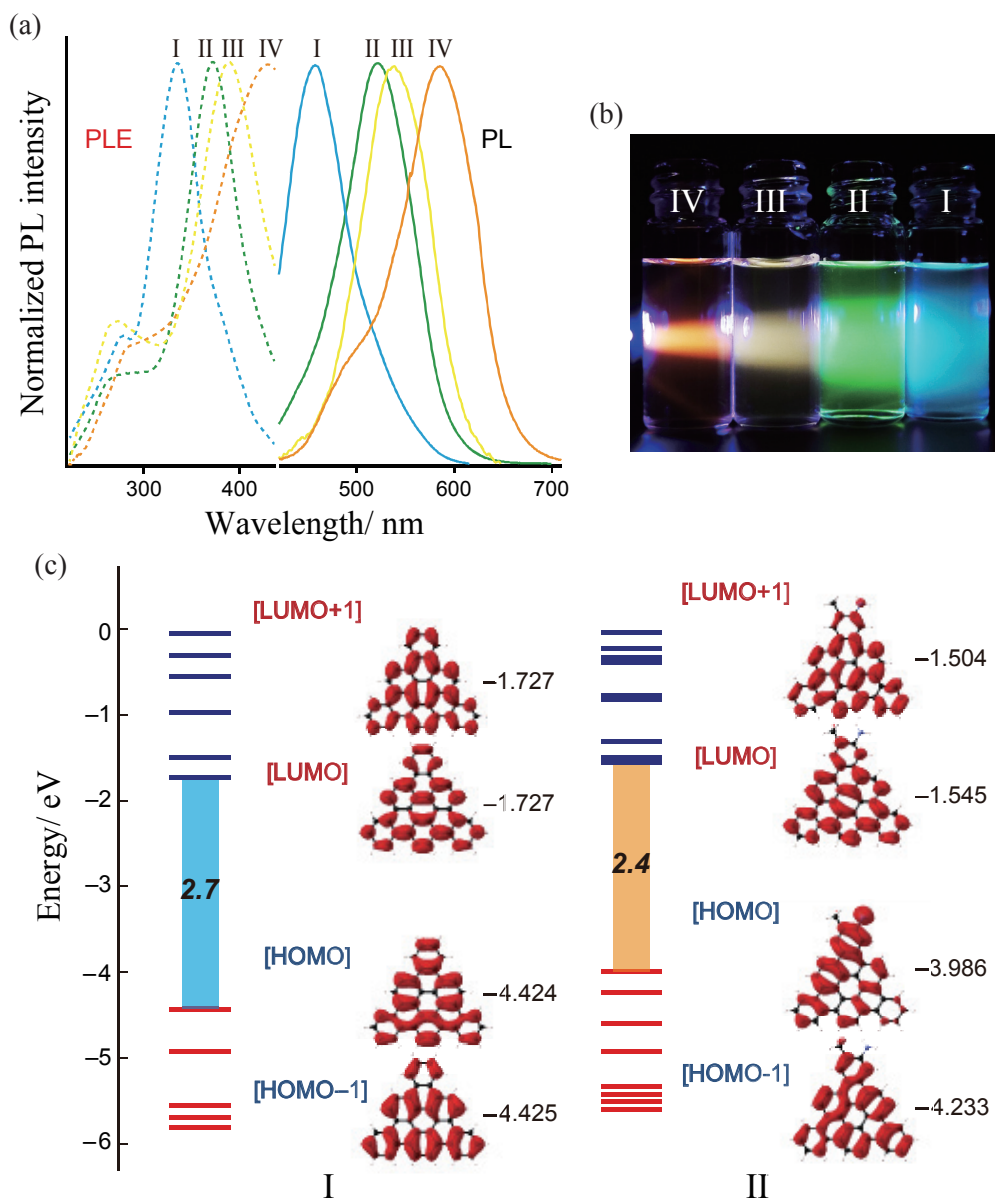
Fig. 4 (a) Normalized PL (solid lines) and PLE (dotted lines) spectra from NGQDs aqueous solutions: I, blue-emitting NGQDs; II, green-emitting NGQDs; III, yellow-emitting NGQDs; IV, orange-emitting NGQDs. (b) Photoluminescence image from NGQDs aqueous solution under excitation using a blue LED (410 nm) from the left side: I, blue-emitting NGQDs; II, green-emitting NGQDs; III, yellow-emitting NGQDs; IV, orange-emitting NGQDs. (c) Energy level diagram of graphene molecules with different functional groups; ab initio calculations were performed using the plane-wave PAW method. Schematic illustrations show the structures used for theoretical calculations. The isosurface presents the HOMO and the lowest unoccupied molecular orbital (LUMO): I, hydrogen-terminated graphene structure; II, -NH$_2$, -CH$_3$ bonded graphene structure.

a strategy for the preparation of NGQDs@CNF-clay hybrid films. The NGQDs@CNFs are self-organized into the space between the positively charged edges of clay particles during drying and are confined tightly by the upper and lower layers of clay platelets in a film. The positive charges of the clay particle edges preferentially attract the negatively charged NGQDs@CNFs, which places the NGQDs@CNFs in the interlayer between

clay platelets and prevent them from aggregation. Characterization of the NGQDs@CNF-clay hybrid film using cross-sectional HRTEM verified a dense coverage of clay platelets with the NGQDs@CNFs between clay particle edges in a strictly planar orientation (Fig. 5(c)), although the NGQDs were not visible due to the high background contrast of the clay platelets. Figure 5(b) shows photographs of the
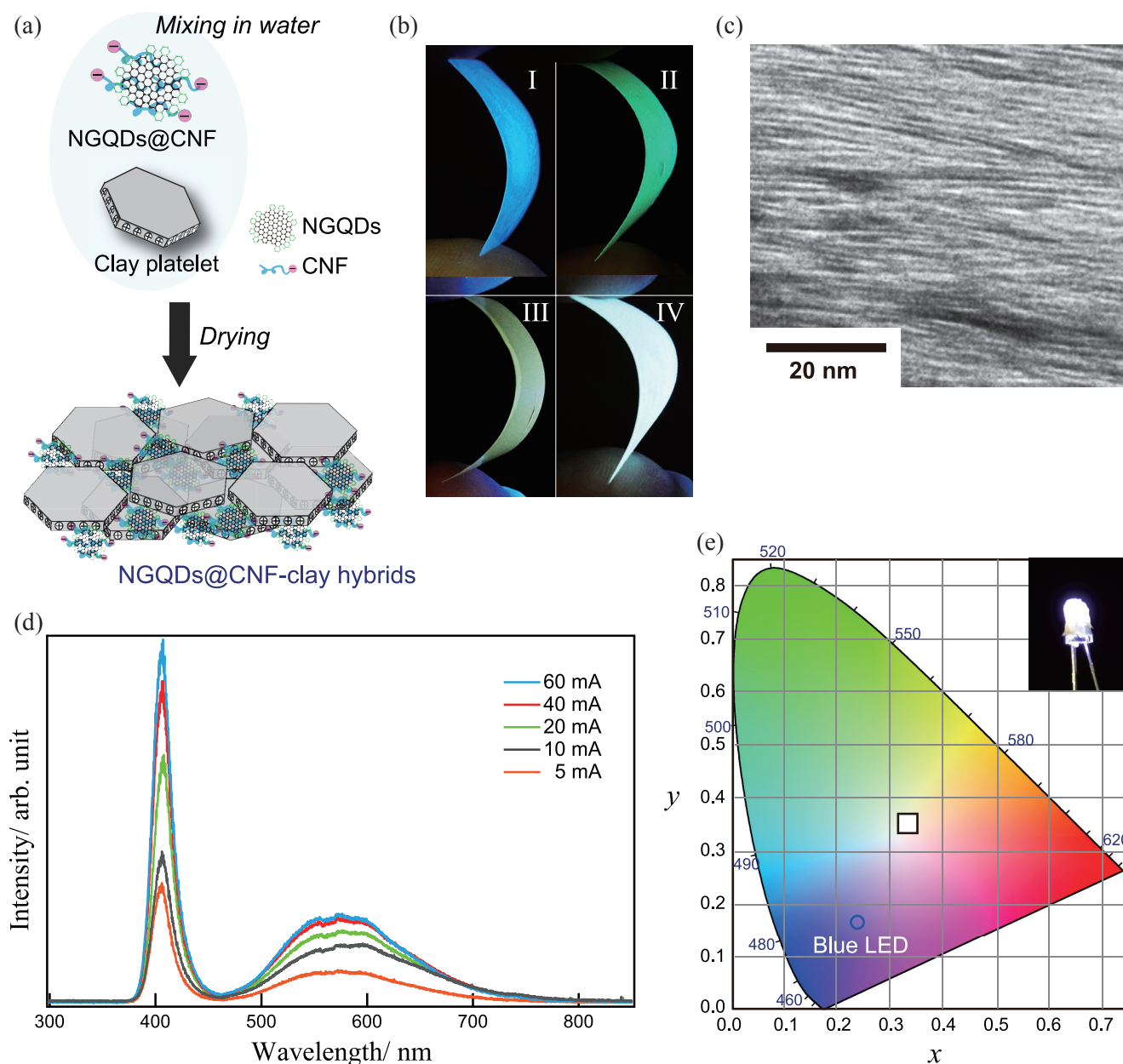
Fig. 5 (a) Schematic illustration of the NGQDs@CNF-clay hybrid preparation process. (b) Photographs of emissions from the NGQDs@CNF-clay hybrid films excited using a UV lamp (365 nm). Each film contains NGQDs with different emission colors: I, blue-emitting NGQDs; II, green-emitting NGQDs; III, yellow-emitting NGQDs; IV, orange-emitting NGQDs. (c) Cross-sectional HRTEM image of NGQDs@CNF-clay hybrid film. (d) EL spectra of GWLED with yellow and orange-emitting NGQDs under various forward currents. (e) CIE coordinates of the blue LED chip and GWLED. The inset shows the white-light emission image from device.

emissions from NGQDs@CNF-clay hybrid films. The NGQDs@CNF-clay hybrid films exhibit strong PL under UV irradiation at 365 nm. These films are highly flexible, and neither aggregation of NGQDs nor phase separation was observed.

Bright multicolor emissions under single-wavelength UV excitation from NGQDs@CNF-clay hybrids make them a novel optical material. The NGQDs@CNF-clay hybrids were used as a light conversion material for white LEDs. The fabrication of GWLEDs was examined using a mixture of NGQDs with yellow and orange emission, where GWLEDs were realized by directly casting NGQDs@CNF-clay hybrid films onto commercial blue LEDs with a 410 nm peak emission. The corresponding electroluminescence (EL) spectra of the GWLEDs under various forward currents are shown in Fig. 5(d). The emission intensity of the underlying blue LED can be tuned by adjusting the amount of NGQDs incorporated in the hybrid film. The emission intensities of both the blue LED and NGQDs@CNF-clay film increased steadily with the forward current to 40 mA and then became saturated at higher current, which demonstrates a GWLED with stable light conversion and color quality. The luminous efficiency was 31.6 lm W^{-1} with a forward current of 20 mA (that of the blue LED chip is 8.9 lm W^{-1}), and a slight decrease was observed when the forward current was increased to 60 mA. This saturation of emission and reduction in efficiency are attributed mainly to the drop in efficiency of the blue LED chip used with increasing forward current and partly to saturation of the NGQD emission. The light conversion (blue-to-NGQDs emission) efficiency was 62.2% with a forward current of 20 mA, which remained almost constant with increasing current. Figure 5(e) shows that the International Commission on Illumination or Commission Internationale de I'Eclairage (CIE) coordinates of the GWLED changed from (0.25, 0.17) for the blue LED to (0.33, 0.37), in which no change of CIE coordinates was observed at different applied currents, which demonstrates the color stability of the output white light.

4. Summary

Novel NGQDs were demonstrated with high PL efficiency and wide tunability of narrow PL lines under single wavelength excitation. The PL energy is controlled according to quantity of edge-functionalization with amino-functional groups. The superior optical properties are expected to enable the use of NGQDs in a large array of future novel applications such as multicolor light-emitting devices, photovoltaics, photodetectors, bioimaging, biosensing, fuel cells, supercapacitors, and hydrogen production. As an example, the NGQDs were incorporated into a flexible and transparent clay host using the electrostatic interactions between cellulose nanofiber (CNF), NGQDs, and clay platelets, and were applied as a color conversion material for blue LEDs to achieve white light emission. The resultant NGQDs@CNF-clay hybrid films exhibit various bright colors under single wavelength excitation without loss of the initial optical properties of the NGQDs. NGQD-based white-LEDs were fabricated by casting the NGQDs@CNF-clay hybrid film onto a blue LED. The NGQD-based white-LED exhibited pure white light emission with CIE coordinates of (0.33, 0.37).

References

(1) Bonaccorso, F., Sun, Z., Hasan, T. and Ferrari, A. C., *Nat. Photon.*, Vol. 4, No. 9 (2010), pp. 611-622.

(2) Loh, K. P., Bao, Q., Eda, G. and Chhowalla, M., *Nat. Chem.*, Vol. 2 (2010), pp. 1015-1024.

(3) Li, Y., Hu, Y., Zhao, Y., Shi, G., Deng, L., Hou, Y. and Qu, L., *Adv. Mater.*, Vol. 23, No. 6 (2011), pp. 776-780.

(4) Gupta, V., Chaudhary, N., Srivastava, R., Sharma, G. D., Bhardwaj, R. and Chand, S., *J. Am. Chem. Soc.*, Vol. 133, No. 26 (2011), pp. 9960-9963.

(5) Zhu, S., Zhang, J., Qiao, C., Tang, S., Tang, Y., Li, Y., Yuan, W., Li, B., Tian, L., Liu, F., Hu, R., Gao, H., Wei, H., Zhang, H., Sun, H. and Yang, B., *Chem. Commun.*, Vol. 47, No. 24 (2011), pp. 6858-6860.

(6) Sun, X., Liu, Z., Welsher, K., Robinson, J. T., Goodwin, A., Zaric, S. and Dai, H., *Nano Res.*, Vol. 1, No. 3 (2008), pp. 203-212.

(7) Pang, D., Zhang, J., Li, Z. and Wu, M., *Adv. Mater.*, Vol. 22, No. 6 (2010), pp. 734-738.

(8) Shen, J., Zhu, Y., Chen, C., Yang, X. and Li, C., *Chem. Commun.*, Vol. 47, No. 9 (2011), pp. 2580-2582.

(9) Kwon, W., Kim, Y. H., Lee, M., Choi, H. C., Lee, T. W. and Rhee, S. W., *Nano Lett.*, Vol. 14, No. 3 (2014), pp. 1306-1311.

(10) Liu, R., Wu, D., Feng, X. and Mullen, K., *J. Am. Chem. Soc.*, Vol. 133, No. 39 (2011), pp. 15221-15223.

(11) Eda, G., Lin, Y. Y., Mattevi, C., Yamaguchi, H., Chen, H. A., Chen, I. S., Chen, C. W. and Chhowalla, M., *Adv. Mater.*, Vol. 22, No. 4 (2010), pp. 505-509.

(12) Gokus, T., Nair, R. R., Bonetti, A., Bohmler, M., Lombardo, A., Novoselov, K. S., Geim, A. K., Ferrari, A. C. and Hartschuh, A., *ACS Nano*, Vol. 3,

No. 12 (2009), pp. 3963-3968.

(13) Galande, C., Mohite, A. D., Naumov, A. V., Gao, W., Ci, L., Ajayan, A., Gao, H., Srivastava, A., Weisman, R. B. and Ajayan, P. M., *Sci. Rep.*, Vol. 1 (2011), Article No. 85.

(14) Tuinstra, F. and Koenig, J. L., *J. Chem. Phys.*, Vol. 53, No. 3 (1970), pp. 1126-1130.

(15) Seredych, M. and Bandoz, T. J., *J. Phys. Chem. C*, Vol. 111, No. 43 (2007), pp. 15596-15604.

(16) Lai, L., Chen, L., Zhan, D., Sun, L., Liu, J., Lim, S. H., Poh, C. K., Shen, Z. and Lin, J., *Carbon*, Vol. 49 , No. 10 (2011), pp. 3250-3257.

(17) Li, Y., Zhao, Y., Cheng, H., Hu, Y., Shi, G., Dai, L. and Qu, L., *J. Am. Chem. Soc.*, Vol. 134, No. 1 (2012), pp. 15-18.

(18) Jiao, L. Y., Wang, X. R., Diankov, G., Wang, H. L. and Dai, H. J., *Nat. Nanotechnol.*, Vol. 5 (2010), pp. 321-325.

(19) Jiao, L. Y., Zhang, L., Wang, X. R., Siankov, G. and Dai, H. J., *Nature*, Vol. 458 (2009), pp. 877-880.

(20) Tetsuka, H., Asahi, R., Nagoya, A., Okamoto, K., Tajima, I., Ohta, R. and Okamoto, A., *Adv. Mater.*, Vol. 24, No. 39 (2012), pp. 5333-5338.

(21) Tetsuka, H., Nagoya, A. and Asahi, R., *J. Mater. Chem. C*, Vol. 3, No. 15 (2015), pp. 3536-3541.

(22) Kresse, G. and Furthmuller, J., *Phys. Rev. B*, Vol. 54, No. 16 (1996), pp. 11169-11186.

(23) Kresse, G. and Furthmuller, J., *Comput. Mater. Sci.*, Vol. 6 , No. 1 (1996), pp. 15-50.

(24) Tetsuka, H., Ebina, T. and Mizukami, F., *Adv. Mater.*, Vol. 20, No. 16 (2008), pp. 3039-3043.

(25) Tetsuka, H., Ebina, T., Nanjo, H. and Mizukami, F., *J. Mater. Chem.*, Vol. 17, No. 33 (2007), pp. 3545-3550.

(26) Tetsuka, H., Ebina, T., Tsunoda, T., Nanjo, H. and Mizukami, F., *Nanotechnology*, Vol. 18, No. 35 (2007), 355701.

(27) Tetsuka, H., Ebina, T., Tsunoda, T., Nanjo, H. and Mizukami, F., *Surf. Coat. Technol.*, Vol. 202, No. 13 (2008), pp. 2955-2959.
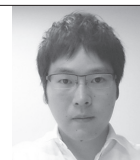
Hiroyuki Tetsuka
  Research Field:
    - Synthesis and Characterization of Graphene Nanostructures
  Academic Degree: Dr.Eng.
  Academic Society:
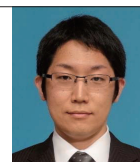   - The Japan Society of Applied Physics

Akihiro Nagoya
  Research Field:
    - First Principles Calculations of Graphene Quantum Dots
  Academic Society:
    - The Physical Society of Japan

Ryoji Asahi
  Research Field:
    - Computational Materials Design for Development of Functional Materials such as Thermoelectrics, Photocatalysts and Photovoltaics.
  Academic Degree: Ph.D.
  Academic Societies:
    - The Japan Society of Applied Physics
    - American Physical Society
    - The Japan Institute of Metals
  Awards:
    - Advanced Technology Award, the Japan Fine Ceramics Association, 2003
    - Corporate Environmental Achievement Award, the American Ceramic Society, 2006
    - Technical Development Award, the Chemical Society of Japan, 2006